PAMM

SPECIAL ISSUE 95th Annual Meeting of the International Association of Applied Mathematics and Mechanics (GAMM)

RESEARCH ARTICLE OPEN ACCESS

Optimization of Shell Structures with Fuzzy Probability-Based Random Fields Using Artificial Neural Networks

Maximilian Schweizer | Marc Fina | Werner Wagner | Steffen Freitag

Institute for Structural Analysis, Karlsruhe Institute of Technology (KIT), Karlsruhe, Germany

Correspondence: Maximilian Schweizer (maximilian.schweizer@kit.edu)

Received: 1 July 2025 | **Revised:** 4 November 2025 | **Accepted:** 25 November 2025

ABSTRACT

The structural design optimization aims for robust structures with minimal use of material resources, leading to slender and thin-walled structures, which entail a higher risk of stability problems. This issue is further influenced by geometrical imperfections, which are subjected to uncertainties. In a common stochastic approach, imperfections can be simulated as random fields with the Karhunen-Loeve-Expansion (KLE) and applied to a finite element (FE) model as geometric deviations. Thus, the probability of a loss of stability can be determined via Monte Carlo Simulation (MCS). To quantify additional epistemic uncertainties within random field simulations, the concept of polymorphic uncertainty modeling is used. In that case, optimization-based interval or fuzzy analyses are required to compute, e.g., imprecise failure probabilities. Numerical calculations of low probabilities require a very large number of samples, resulting in high computation times. In order to reduce the computation time, a surrogate model based on Artificial Neural Networks (ANNs) is developed to replace the FE buckling analysis for the polymorphic uncertainty analysis. The basic idea is to use the random numbers of the KLE series as inputs for the ANN. In the training process, the training samples are computed by a geometrical nonlinear FE model. After successful training, the surrogate model is able to predict the buckling load with negligible computation time of the MCS, compared to the computationally demanding FE model. The main novelty of the presented method is an ANN surrogate model for random field-based FE buckling analysis used to perform optimization tasks considering polymorphic uncertainties.

1 | Introduction

Design optimization leads to slender and thin-walled structures, which entail a higher risk of stability problems and high sensitivity to geometrical imperfections. Since imperfections are of random nature, they should be considered probabilistically [1–4]. In this paper, imperfections are modeled as random fields with the Karhunen-Loeve-Expansion (KLE) method [5–7]. Imperfection modeling with random fields in buckling analysis has been widely investigated in, e.g., [5, 8]. The consideration of epistemic uncertainty of the correlation parameters of the random field, leading to fuzzy probability-based random fields in numerical buckling analysis, is introduced in [9–14]. The lack of an analytical solution and thus, running Monte-Carlo simulations with complex FE models (FE-MCS), causes high computation times. This issue becomes increasingly problematic as more variables are added to the model, as in the case of design optimization with polymorphic uncertainties, see e.g., [15–17] for a reinforced concrete bridge. In this paper, the optimization problem with polymorphic uncertainties is considered in two categories: constraint optimization, see e.g., [18] for a wooden bridge, and multi-objective optimization, see e.g., [19] for a glulam beam and [20, 21] for shell structures. Multi-objective optimization is widely discussed in, e.g., [22–27].

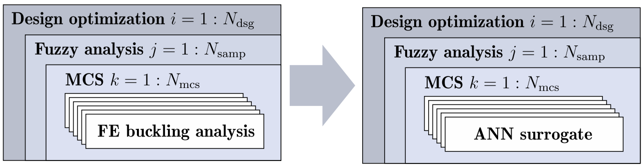

FIGURE 1 | Triple-loop algorithm with ANN surrogate model replacing the FE buckling analysis.

In order to reduce the computational effort, surrogate models replace the basic solution by approximating the relationship between input and output variables. Some examples for the application of surrogate models in structural engineering problems considering uncertainties are: multilevel surrogate modeling for optimization with polymorphic uncertain parameters [15], bounding failure probabilities in imprecise stochastic FE models [28], structural response prediction of buildings [29–31], uncertain pedestrian load modeling in footbridge design [32] and the Control-Variates method in shell buckling [33–35]. ANN-based surrogate models for the prediction of buckling loads without random fields but with material and structural parameters as input variables have already been used, see e.g., [36, 37]. ANNs with random field inputs are already been developed, e.g. in geotechnical engineering [38, 39]. In [40], a convolutional neural network is applied to process the geometrical imperfections as image input to predict the buckling load of a cylindrical shell. In a preliminary work [41], the random field variables are used as input for an ANN to predict the buckling load of structures with geometrical imperfections. However, a surrogate model to take into account design, fuzzy, and random field variables in the framework of structural design optimization with polymorphic uncertainty has not been investigated yet. In this contribution, the surrogate model introduced in [41] is extended to capture additional fuzzy parameters and structural design variables, and used in design optimization of a fiber composite plate structure considering polymorphic uncertainties. The computational model consists of a triple-loop algorithm (design optimization, fuzzy analysis, and MCS), see Figure 1.

The design optimization of a structure under consideration of polymorphic uncertainty is not trivial, because adequate surrogate measures for the uncertain objective function and the uncertain constraints are required. In this contribution, two optimization tasks are presented: multi-objective and constraint optimization. The computational benefit of the surrogate model is demonstrated with a numerical example of a fiber composite panel by optimizing the thickness and the fiber angle.

2 | Fuzzy Probability-Based Random Fields

In this paper, geometrical imperfections are modeled as fuzzy probability-based correlated random fields applied to an FE model of the structure as stress-free displacements. The basics of the random field theory and the KLE method are briefly summarized based on [42, 43]. Given the surface of a structure as domain Ω and the location vector $\boldsymbol{x}$, the geometric deviations $w(\boldsymbol{x})$ are assumed to be random and, therefore, modeled as correlated random field. A random field $w(\boldsymbol{x}, \theta)$ is a scalar field that assigns a random value at each point $\boldsymbol{x} \in \Omega$ and for each event $\theta \in \Theta$, where Θ is the set of possible events. Thus, a random field is a set of random variables

$$\{w(\boldsymbol{x}, \theta) \mid \boldsymbol{x} \in \Omega, \theta \in \Theta\} \ . \tag{1}$$

For the numerical implementation into an FE model, the random field is discretized according to the FE nodes. The random field is modeled with the Karhunen-Loeve-Expansion (KLE) method, introduced in [44], which is a series expansion method based on the spectral decomposition of its covariance function

$$C(\boldsymbol{x}_i, \boldsymbol{x}_j) = \sigma^2 \rho(\boldsymbol{x}_i, \boldsymbol{x}_j) \tag{2}$$

with standard deviation σ and autocorrelation function $\rho(\boldsymbol{x}_i, \boldsymbol{x}_j)$. Evaluating ρ for each pair of points $(\boldsymbol{x}_i, \boldsymbol{x}_j) \in \Omega$, the autocorrelation matrix

$$\boldsymbol{R} = \begin{bmatrix} \rho(\boldsymbol{x}_1, \boldsymbol{x}_1) & \dots & \rho(\boldsymbol{x}_1, \boldsymbol{x}_N) \\ \vdots & \ddots & \vdots \\ \rho(\boldsymbol{x}_N, \boldsymbol{x}_1) & \dots & \rho(\boldsymbol{x}_N, \boldsymbol{x}_N) \end{bmatrix} \tag{3}$$

is obtained, where N is the total number of FE nodes. The deterministic functions used to expand any realization of the field $w(\boldsymbol{x}, \theta_0)$, are determined by solving the eigenvalue problem of the autocorrelation matrix

$$\boldsymbol{R}\boldsymbol{\varphi}_i = \lambda_i \boldsymbol{\varphi}_i \ \ , \tag{4}$$

which is symmetric and positive definite. Thus, the discrete random field is written as

$$\hat{w}(\boldsymbol{x}, \theta) = \mu + \sigma \sum_{i=1}^{N} \xi_i(\theta) \sqrt{\lambda_i} \varphi_i(\boldsymbol{x}) \ \ , \tag{5}$$

where $\xi_i(\theta)$ is a standard normal distributed random variable $\xi_i(\theta) \sim \mathcal{N}(0, 1)$. As the random field is used to describe the deviations with respect to an ideal structure without imperfections $\hat{w}(\boldsymbol{x}) = 0$, the mean value is set to zero $\mu = 0$. For the autocorrelation function $\rho(\boldsymbol{x}_i, \boldsymbol{x}_j)$, a quadratic exponential function is used

$$\rho(\boldsymbol{x}_i, \boldsymbol{x}_j) = \exp\left(-\frac{d^2(\boldsymbol{x}_i, \boldsymbol{x}_j)}{\ell_c^2}\right) \quad \text{with} \quad d(\boldsymbol{x}_i, \boldsymbol{x}_j) = |\boldsymbol{x}_i - \boldsymbol{x}_j| \tag{6}$$

where ℓ_c is the correlation length and d is the distance between two FE nodes. In this paper, the mean value $\mu = 0$ and the standard deviation σ are constant within the domain Ω. The autocorrelation function ρ is only dependent on the distance $d(\boldsymbol{x}_i, \boldsymbol{x}_j)$ and the correlation length ℓ_c. Therefore, the random field is homogeneous. Further, the random field is completely defined by its mean value μ, standard deviation σ and autocorrelation function ρ. Thus, it is referred to as Gaussian random field. The eigenvalues λ_i of the autocorrelation matrix according to Equation (4) can be sorted in a descending order converging to zero. Truncating the series in Equation (5) after the n-th term yields the approximated random field. The required number n of eigenvalues to be considered in the KLE can be determined with

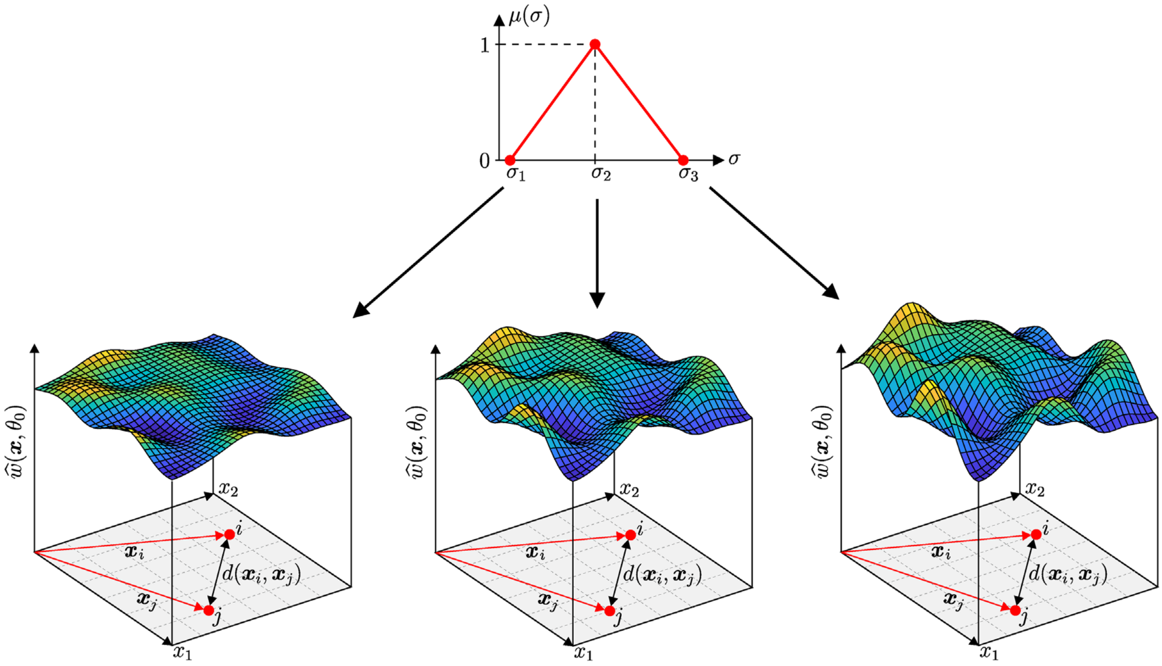

FIGURE 2 | Fuzzy standard deviation $\tilde{\sigma}$ with an example of a random field realization with a correlation length of $\ell_c = 300$ and three different standard deviations.

the quality index, given in [45]

$$Q = \frac{1}{\mathrm{tr}(\boldsymbol{C})} \sum_{k=1}^{n} \lambda_k \quad . \tag{7}$$

In most cases a quality index of $Q = 0.99$ is used [8]. The decrease of sorted eigenvalues λ_i of the autocorrelation matrix depends on the correlation length ℓ_c. The higher the correlation length ℓ_c, the higher is the decrease rate of the eigenvalues λ_i and thus, the number of KLE-terms decreases.

In Figure 2, three examples of two-dimensional random field realizations are presented. A fuzzy probability-based random field (fp-r field) is obtained by modeling at least one of the random field parameters as fuzzy variable [9, 46]. The definition of a fuzzy variable is briefly summarized based on [47, 48]. In the fuzzy-set-theory, the membership of an element x to a set A is rated gradually with a membership function $\mu_A(x)$. The normalized fuzzy variable $\tilde{A}$ is defined as

$$\tilde{A} = \{(x, \mu_A(x)) | x \in \mathbb{R}\}, \quad \mu_A(x) : \mathbb{R} \to [0, 1] \quad . \tag{8}$$

In this paper, the standard deviation of the random field is modeled as a fuzzy triangular number, which is convex and has a membership function with two linear parts, described by the following notation: $\tilde{\sigma} = \langle \sigma_1 \; \sigma_2 \; \sigma_3 \rangle$. The fuzzy standard deviation $\tilde{\sigma}$ is inserted in Equation (5) to obtain the fp-r field.

3 | Buckling Analysis of Geometrically Imperfect Structures with Polymorphic Uncertainty

The buckling analysis introduced in this section is based on [34, 49]. At the critical buckling load level, the structure is in an indifferent equilibrium state, and the tangential stiffness matrix $\boldsymbol{K}_T$ is singular. In order to find a stability point, it can be distinguished between linear and nonlinear buckling analysis. For structures with linear pre-buckling behavior, the linear buckling analysis is sufficient, which is based on the decomposition of the tangent stiffness matrix

$$\boldsymbol{K}_T = \boldsymbol{K}_{\mathrm{lin}} + \boldsymbol{K}_{\mathrm{nlin}} \quad , \tag{9}$$

where the stiffness matrix is divided into linear $\boldsymbol{K}_{\mathrm{lin}}$ and nonlinear $\boldsymbol{K}_{\mathrm{nlin}}$ parts. With an external load $\boldsymbol{P}_0$, the displacements $\boldsymbol{u}_0$ can be calculated with the linear solution

$$\boldsymbol{K}_T(\boldsymbol{0})\boldsymbol{u}_0 = \boldsymbol{P}_0 \quad \Longleftrightarrow \quad \boldsymbol{u}_0 = \boldsymbol{K}_T(\boldsymbol{0})^{-1}\boldsymbol{P}_0 \quad , \tag{10}$$

with $\boldsymbol{K}_T(\boldsymbol{0}) = \boldsymbol{K}_{\mathrm{lin}}$. The linear buckling analysis consists of the solution of the eigenvalue problem

$$[\boldsymbol{K}_{\mathrm{lin}} + \Lambda \boldsymbol{K}_{\mathrm{nlin}}(\boldsymbol{u}_0)]\boldsymbol{\varphi} = \boldsymbol{0} \quad , \tag{11}$$

which leads to a critical buckling load factor Λ_{cr} and the initial postbuckling mode $\boldsymbol{\varphi}$. The critical buckling load with the corresponding critical displacement can be calculated by

$$\boldsymbol{P}_{\mathrm{cr}} = \Lambda_{\mathrm{cr}} \boldsymbol{P}_0 \quad , \quad \boldsymbol{u}_{\mathrm{cr}} = \Lambda_{\mathrm{cr}} \boldsymbol{u}_0 \quad . \tag{12}$$

The load-displacement curves are computed with the displacement controlled Newton-Raphson method in the Finite Element Analysis Program FEAP [50]. Considering polymorphic uncertainty in the input parameters, the outputs become fuzzy probability distributions. Given an external load (E) and the load resistance (R), the load bearing capacity limit state is defined as $g = R - E = 0$, where the resistance is the critical load of the imperfect structure $R = P_{\mathrm{cr,imp}}$. Thus, the fuzzy probability distribution of the limit state can be calculated. The fuzzy stochastic quantities of interest considered in this contribution

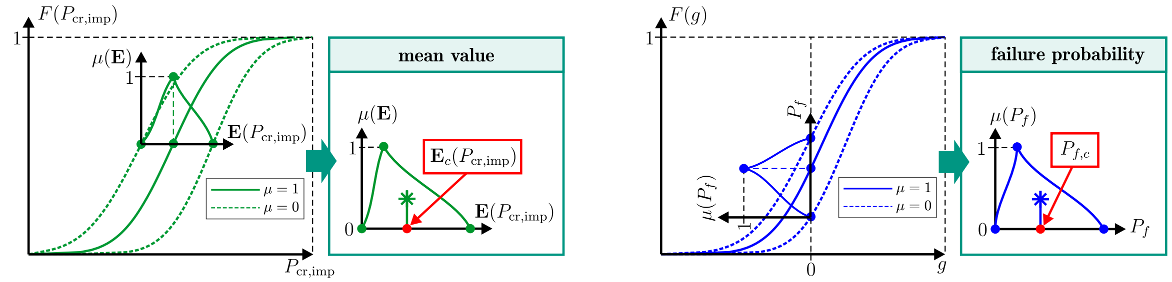

FIGURE 3 | Fuzzy CDFs and centroids of the fuzzy stochastic outputs. Critical load and mean value (left), limit state and failure probability (right).

are: failure probability, mean value, and coefficient of variation of the critical load. For the optimization process, the fuzzy stochastic quantities have to be reduced to deterministic values [27], by information reduction measures (IRM), see e.g., [51]. Here, the centroids of the fuzzy stochastic quantities of interest are used as IRM and are marked with index "c". In Figure 3, the fuzzy cumulative distribution functions (CDFs) and the centroids of the fuzzy stochastic outputs are visualized.

4 | Structural Design Optimization with Polymorphic Uncertainty

The standard form of an optimization problem is defined as minimization problem with constraints by convention [52]. In this paper, the minimization problem with inequality constraint is given by

$$\text{minimize } f(\boldsymbol{x_d}), \quad \boldsymbol{x}_d \in \mathcal{D}, \quad \text{subject to: } h(\boldsymbol{x_d}) \leq b\,. \tag{13}$$

where $f : \mathbb{R}^n \mapsto \mathbb{R}$ is the objective function to be minimized, $\boldsymbol{x_d}$ is the vector of design variables in the domain $\mathcal{D}$, h is the constraint function, and b is a threshold value. A maximization problem can simply be converted into a minimization problem by negating the objective function. In general, the structural design optimization aims for a high load bearing capacity with the lowest possible material consumption. In a deterministic approach, this would be the maximization of the buckling load while minimizing the mass. Taking polymorphic uncertainty into account, the buckling load is a fuzzy probability distribution and thus, the formulation of the optimization problem is not evident, but offers many possibilities. Depending on the fuzzy stochastic quantity of interest, the problem is divided into two categories: multi-objective optimization and constraint optimization.

Multi-objective optimization arises from the consideration of more than one objective, such as performance and robustness. Robustness is the ability of a structure to consistently maintain optimal performance under fluctuating conditions [53]. Robustness versus performance optimization with polymorphic uncertainty is investigated, e.g., in [21, 27]. In this paper, the centroid of the fuzzy coefficient of variation $CV_c(P_{\text{cr,imp}})$ is a robustness measure, and the centroid of the fuzzy mean value of the critical load $\mathbf{E}_c(P_{\text{cr,imp}})$ is a performance measure. Utilizing the IRMs, the multi-objective optimization is formulated as:

$$\text{minimize } [CV_c(P_{\text{cr,imp}})\,,\ -\mathbf{E}_c(P_{\text{cr,imp}})], \quad \boldsymbol{x}_d \in \mathcal{D}\,. \tag{14}$$

These two objectives are often conflicting, as they are not satisfied at the same design point. In that case, a Pareto front can be helpful to find a compromise between the two objectives [21, 23–25]. In multi-objective optimization, a solution is said to be Pareto optimal if no objective can be improved without degrading at least one other objective [26]. The set of all Pareto optimal solutions forms the Pareto front.

The constrained optimization arises from the need to ensure both reliability and economy. In reliability analysis, according to Eurocode [54], the failure probability has to be lower than a specific threshold value based on the consequence class. As an example in this paper, the threshold value is set to 10^{-4}. This information is used as a constraint while minimizing the material consumption of the structure. The constraint optimization is formulated as:

$$\text{minimize volume}(\boldsymbol{x}_d), \quad \boldsymbol{x}_d \in \mathcal{D}, \quad \text{subject to: } P_{f,c} \leq 10^{-4}\,. \tag{15}$$

In this paper, a composite plate structure with constant material density is investigated, and thus, minimizing the volume of the structure is equivalent to minimizing the mass. In this way, an economic design is achieved while ensuring a low failure probability.

5 | Computational Model

The overall computational model consists of a triple-loop algorithm, represented in Figure 4 for two design variables x_1 and x_2. The design input space is discretized in equidistant design sample points, which are used to search for the optimal solutions, i.e., a discrete optimization problem. At each design sample point, the fuzzy stochastic analysis (FSA) is applied to calculate the fuzzy stochastic output. Therefore, the fuzzy input variable x is discretized in alpha-levels [55]. At the bottom alpha-level ("support"), the fuzzy input space is discretized in equidistant fuzzy sample points. At each fuzzy sample point, an MCS with $N_{\text{samp}}^{\text{mcs}}$ samples is performed, using the ANN surrogate model, to obtain the solution for the stochastic output z. Thus, a least squares (LSQ) polynomial surrogate model is built, denoted by $\widehat{\mathcal{M}}(x)$. At each alpha level, the minimum and the maximum value of the output are computed via particle swarm optimization (PSO) by using the LSQ-polynomial surrogate model, yielding the left bounds $\hat{z}_{\alpha_{k,l}}$ and the right bounds $\hat{z}_{\alpha_{k,r}}$ for the membership function of the fuzzy stochastic output variable. By this procedure, the discrete membership function of the output variable $\mu(z)$ is obtained. Afterwards, the centroid of the area under the

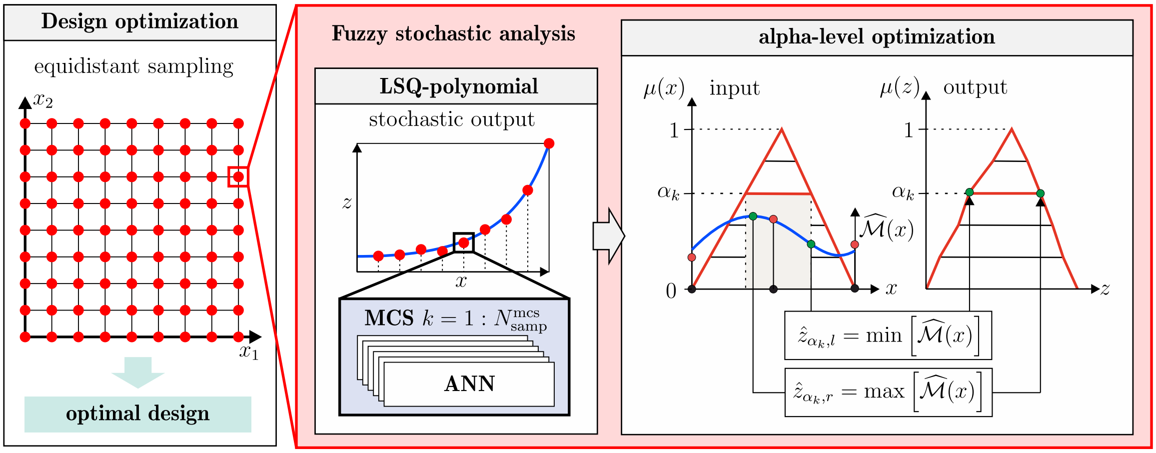

FIGURE 4 | Computational model for design optimization and fuzzy stochastic analysis.

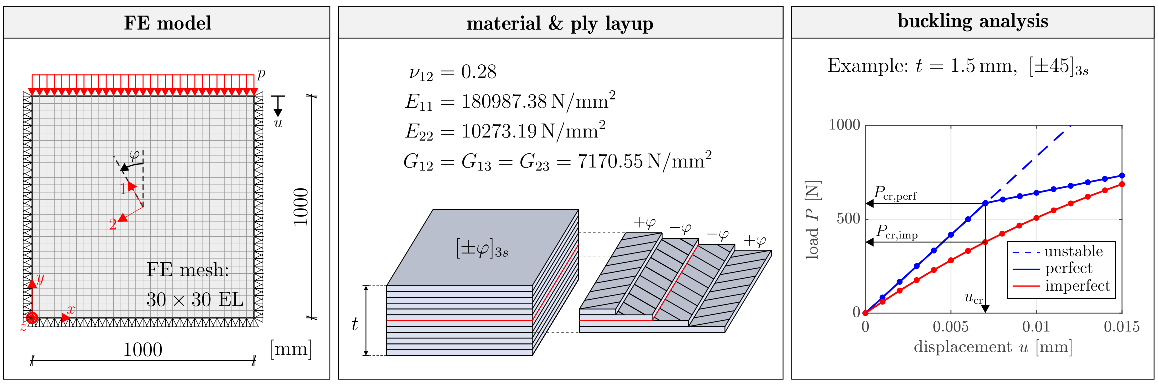

FIGURE 5 | FE model of the fiber composite plate, ply layup, material parameters and load-displacement curves.

membership function is calculated with the trapezoidal rule. In total, two surrogate models (ANN and LSQ) are used in the FSA to calculate the centroids of the fuzzy stochastic outputs of interest, i.e., mean value, coefficient of variation and failure probability.

6 | Example

In this example, the design parameters of a fiber composite plate are optimized, Figure 5 (left). The classical composite panel of thickness t consists of transversally isotropic material with 12 layers and straight fibers, see Figure 5 (middle). The fiber orientation φ is alternating and symmetrical, which is designated with the notation $[\pm\varphi]_{3s}$ according to [21, 56]. The top edge of the structure is loaded with a line load p. For the load-displacement curves and for the critical loads, the load is calculated as resultant: $P = p \cdot 1000\text{mm}$. The external load is assumed to be normally distributed $P \sim \mathcal{N}(100, 10)[\text{N}]$. The structure with and without random imperfections is referred to as "imperfect" and "perfect" structure, respectively. The corresponding load-displacement curves are depicted in Figure 5 (right). The perfect structure follows the primary (unstable) path, represented with a dashed line. For the visualization of the load-displacement curve, the first eigenmode with an amplitude of 1 mm is applied to the structure as an imperfection at the stability point to deflect the structure into the secondary (stable) path. The load and displacement values at the stability point are $P_{\text{cr,perf}}$ and u_{cr}. For the imperfect structure, a Gaussian random field with correlation length of $\ell_c = 500\text{mm}$, mean value $\mu = 0$ and standard deviation of $\sigma = 1\text{mm}$ is used for the shape of the structural surface. The imperfect structure follows a non-linear load-displacement curve and has no stability point, see Figure 5. Therefore, the evaluation point for the critical buckling load of the imperfect structure $P_{\text{cr,imp}}$ is defined as $P_{\text{cr,imp}}(u_{\text{cr}})$, i.e., the load level at the critical displacement u_{cr} of the perfect structure, according to [8, 9, 57]. The critical displacement u_{cr} has to be updated at each design sample point during the optimization process. In this paper, a parameter study for the correlation length in the range $\ell_c = [300,\ 500]\,\text{mm}$ is conducted. The standard deviation is modeled as a fuzzy triangle number $\sigma = \langle 0.5\ 1.0\ 1.5 \rangle[\text{mm}]$. Exemplary realizations of random fields are presented in Figure 6. In [21], the same structure but with tow-steered fiber path has been optimized with multi-objective optimization, considering aleatory and epistemic uncertainties separately. In this contribution, polymorphic uncertainty and the failure probability as a constraint are taken into account.

The design input space is discretized in $N_{\text{samp}}^{\text{dsg}} = 19 \times 19 = 361$ equidistant design sample points. The FSA is done at each design sample point using an LSQ-polynomial of the sixth degree with $N_{\text{samp}}^{\text{fuzzy}} = 11$ fuzzy sample points at the support of the fuzzy input variable. At each fuzzy sample point an MCS with $N_{\text{samp}}^{\text{mcs}} = 10^6$

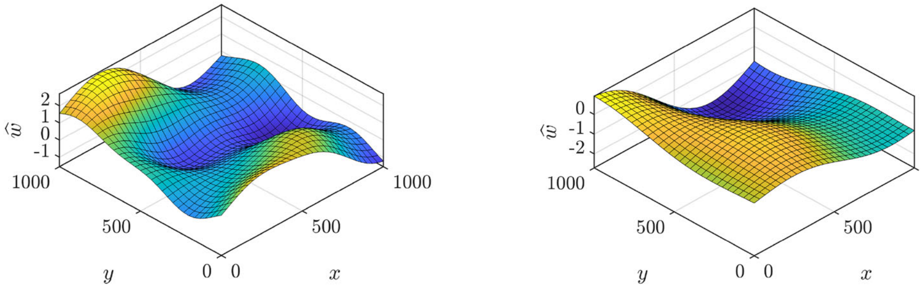

FIGURE 6 | Exemplary realizations of random fields with a standard deviation of $\sigma = 1$ and correlation lengths of $\ell_c = 300$ mm (left) and $\ell_c = 500$ mm (right).

samples is performed. The FSA yields the centroids of the fuzzy stochastic outputs of interest, i.e., mean value, coefficient of variation, and failure probability. The high numbers of fuzzy sample points and MC samples are required to compute failure probabilities of approximately 10^{-4}. In this example, the total number of realizations is given by

$$N_{\text{samp}} = N_{\text{samp}}^{\text{dsg}} \cdot N_{\text{samp}}^{\text{fuzzy}} \cdot N_{\text{samp}}^{\text{mcs}} = 361 \cdot 11 \cdot 10^6 = 3.971 \cdot 10^9 \,. \tag{16}$$

This corresponds to the number of required FE realizations, if just the LSQ surrogate model within the fuzzy analysis and no surrogate model within the MCS were applied. Thus, the requirement of a further surrogate model for the MCS is evident.

6.1 | ANN Training

With a correlation length of $\ell_c = 500$mm and a quality index of $Q = 0.99$, the KLE requires 12 random input variables. Including the fuzzy standard deviation $\sigma = \langle 0.5\ 1.0\ 1.5\rangle$[mm] and the two design variables t (thickness) and φ (fiber orientation angle), the surrogate model has 15 input variables in total. The surrogate model is a feed-forward neural network (FNN), and the network architecture is calibrated with the lowest investigated correlation length ℓ_c because this corresponds to the maximal number of input variables. It has been found that five hidden layers with 20 neurons in each one are sufficient. For the training procedure, the input data is generated with two different sampling distributions: the uniform distribution for design and fuzzy variables, and the standard normal distribution for the random variables ξ_i, because they are standard normal distributed in the KLE. The target samples are generated via FE-MCS with $N_{\text{target}} = 10^5$ samples. The ANN training procedure is represented in Figure 7. The training is conducted five times with the same training data in order to investigate the surrogate model uncertainty. After training, the response functions are plotted and compared with the FE solution for plausibility control, see Figure 8. The response surface for the design variables is calculated with $10 \times 10 = 100$ grid sample points and plotted in Figure 8 (left). The five ANN solutions are visualized as continuous lines for the fuzzy standard deviation, see Figure 8 (middle), and the random variable ξ_1, see Figure 8 (right). For those two response function plots, the FE solution is calculated with 7 sample points for each one. The response functions for the random variables ξ_i obtained by the KLE are widely discussed in [41]. This provides valuable insights about the influence of certain variables on the output function.

In this case, it is clearly visible that $P_{\text{cr,imp}}$ is monotonically increasing with respect to t, which is intuitive. On the other hand, the influence of the fiber angle φ is not monotonic and shows local maxima at $\varphi = 25°$ and $\varphi = 80°$. This information can be used as an indication for optimal design points. A further plausibility control is the computation of the fuzzy CDF of the limit state function g at the midpoint of the design space, see Figure 9, which is calculated with 10^4 samples and shows a good approximation. The total number of FE simulations required to train and validate the surrogate model is given by the target samples and the testing samples. The utilized number of target samples $N_{\text{target}} = 10^5$ might seem to be expensive, but considering the number of realizations N_{samp} in Equation (16), the numerical benefit is mainly defined by the FE simulation reduction factor

$$f_{\text{red}} = \frac{N_{\text{samp}}}{N_{\text{target}} + N_{\text{test}}} = \frac{3.971 \cdot 10^9}{10^5 + 10^4 + 114} \approx 3.6 \cdot 10^4 \,. \tag{17}$$

6.2 | Multi-Objective Optimization

As introduced in Section 4, the two considered objective functions are the centroid of the fuzzy mean value and the centroid of the fuzzy coefficient of variation of the critical buckling load $P_{\text{cr,imp}}$ and are plotted in Figure 10 (left). The mean value shows a similar behavior as the response function in Figure 8. It is particularly noticeable that both the mean value and the standard deviation have monotonous dependency to the thickness t, where $\mathbf{E}_c(P_{\text{cr,imp}})$ is increasing, and $CV_c(P_{\text{cr,imp}})$ is decreasing with t. As the objectives are maximization of $\mathbf{E}_c(P_{\text{cr,imp}}))$ and minimization of $CV_c(P_{\text{cr,imp}})$, all optimal points are located at the upper bound of t, which is $t = 2$mm in this case and the dimension of the optimization problem could be reduced to just one design variable φ. Therefore, it is practical to view the one-dimensional objective functions at $t = 2$mm with respect to φ, see Figure 10 (center). The objectives are not conflicting with respect to t, but are conflicting with respect to φ. The optimal points $\max(\mathbf{E}_c(P_{\text{cr,imp}}))$ and $\min(CV_c(P_{\text{cr,imp}}))$ are located at $\varphi = 30°$ and $\varphi = 75°$, respectively. For those two design points, the fuzzy CDFs of the limit state function are presented in Figure 10 (bottom-right). The two probability distributions are very different from each other but both solutions have a similarly low probability of failure $F(g = 0)$ with $P_{f,c} < 10^{-7}$. All 361 feasible solutions are represented as blue dots in Fig. 10 (top-right). Through discrete searching of the Pareto-optimal solutions, the Pareto-front is determined and visualized as a red line. It represents the optimal trade-offs between the two objectives. This optimization is repeated

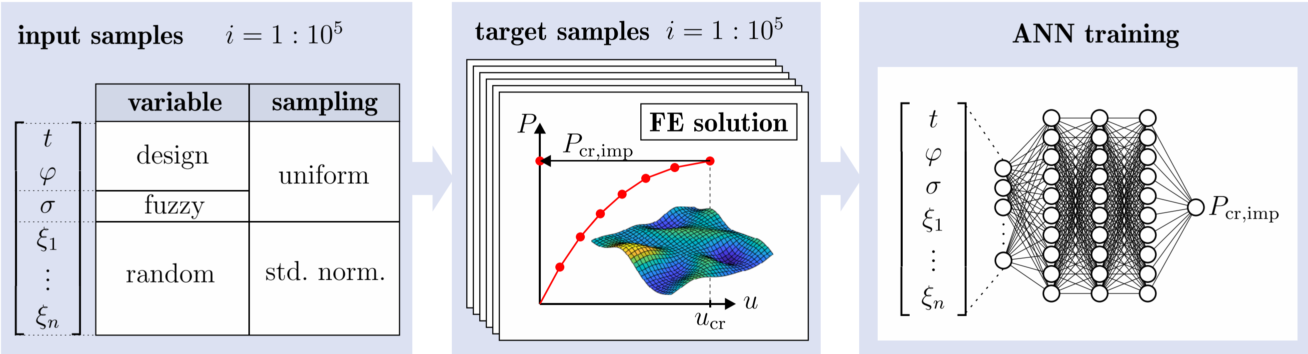

FIGURE 7 | ANN training procedure.

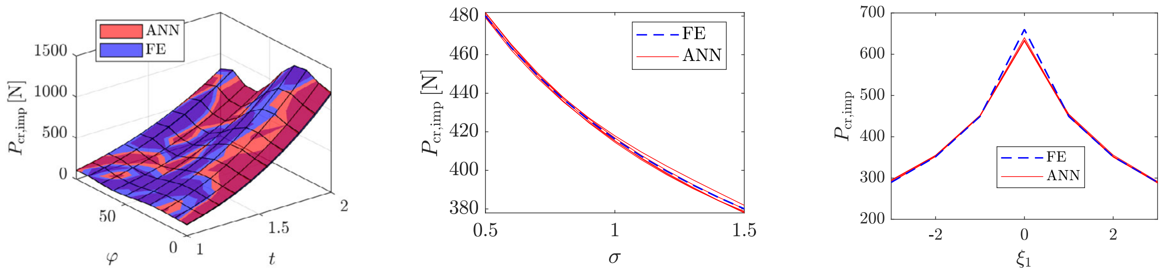

FIGURE 8 | Plasibility control: comparison of response functions of varying input variables.

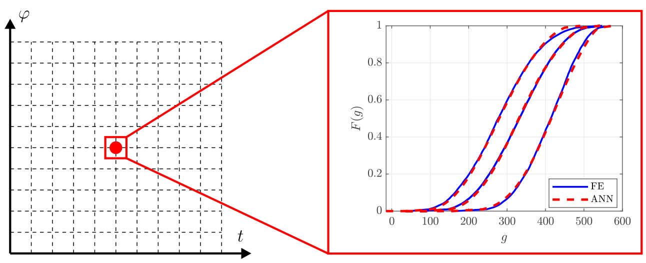

FIGURE 9 | Plausibility control: CDF of the limit state function for a selected design.

for three different correlation lengths $\ell_c = \{300, 400, 500\}$, see Figure 11. The Pareto-optimal solutions remain at the same fiber angle for different correlation lengths. In order to make a final decision, priorities must be set regarding performance versus robustness, or a compromise solution can be achieved by weighting both objectives accordingly.

6.3 | Constraint Optimization

The objective is to minimize the volume, subject to the constraint of $P_{f,c} < 10^{-4}$. In this case, the objective function is trivial, as the volume is linearly increasing with respect to the thickness t and constant with respect to the fiber angle φ. The centroid of the fuzzy failure probability $P_{f,c}$ is depicted in Figure 12. The intersection with the threshold plane at $P_{f,c} = 10^{-4}$ implicitly defines an isoline as boundary of the feasible design space. As the objective and the constraint function are monotonically increasing and decreasing with respect to t, the optimal solution is located on the lower bound of the objective function, i.e., the constraint isoline. Thus, the isoline is plotted on the objective function in Figure 12 (middle). The minimization of the volume subject to the constraint, results in the optimal solution of $\varphi = 80°$ and $t = 1.32$ mm. The same optimization procedure is repeated for different correlation lengths. The constraint isolines are plotted in Figure 12 (right), resulting in the optimal solutions in the range of $\varphi = [75\ 80]$. At the optimal design point with a correlation length of $\ell_c = 500$ mm, a convergence plot of the failure probability is depicted in Figure 13 (left). It clarifies the requirement of high sample numbers N_{mcs} for the calculation of a low probability. In Figure 13 (right), the converged fuzzy failure probability with $N^{\mathrm{mcs}}_{\mathrm{samp}} = 10^6$ shows that the centroid is slightly lower than the threshold and therefore, fulfills the constraint. However, the membership function of the fuzzy failure probability $\mu(P_f)$ also has values in the failure domain. If the complete fuzzy membership function should be below the threshold, the upper bound of the support must be used as an information reduction measure instead of the centroid. However, this would lead to a higher thickness and a higher material consumption. On the other hand, the fuzziness of the standard deviation of the fuzzy random field could be reduced by further investigations, i.e., measurements. The presented concept is a compromise between a reliable and economic design. For a comparison of the results, the centroids of the fuzzy mean value $\mathbf{E}_c(P_{\mathrm{cr,imp}})$ and the centroids of the fuzzy coefficient of variation $CV_c(P_{\mathrm{cr,imp}})$ are given in Table 1 for the optimal designs. The correlation length has no significant influence on the optimal fiber orientation design. More important is the consideration of the quantity of interest. Robustness and reliability are matched at $\varphi \approx 75°$, while the optimal performance is found at $\varphi = 30°$. This demonstrates how the consideration of different quantities of interest can significantly affect the optimal design of the fiber orientation in fiber composite structures.

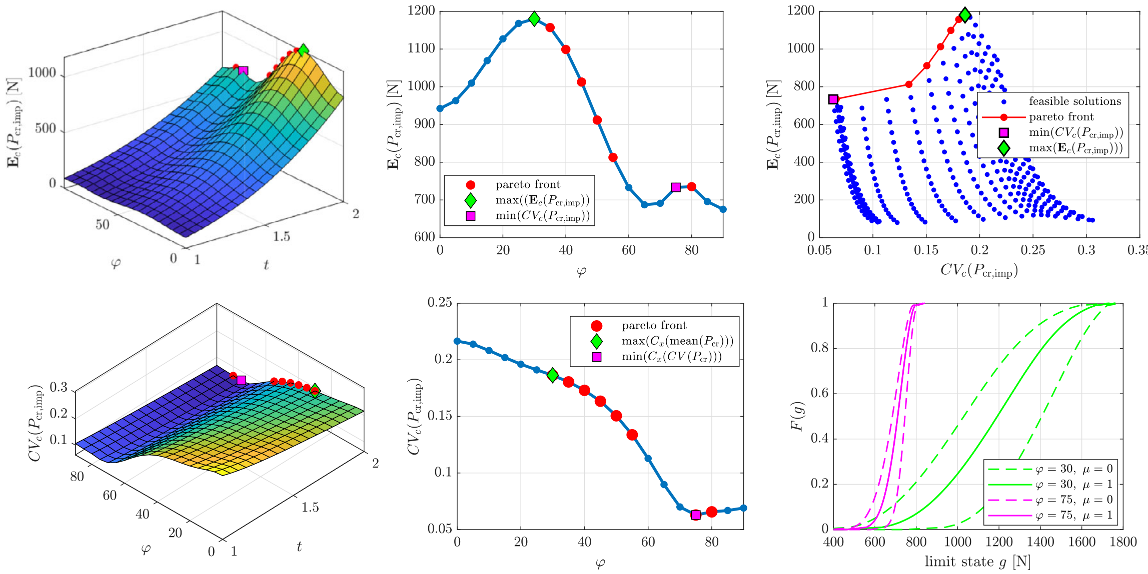

FIGURE 10 | Centroid of the fuzzy mean value: 2D (top left) and 1D (top middle), centroid of the fuzzy coefficient of variation: 2D (bottom left) and 1D (bottom middle). Pareto front (top right) and fuzzy CDFs for two Pareto optimal solutions (bottom right).

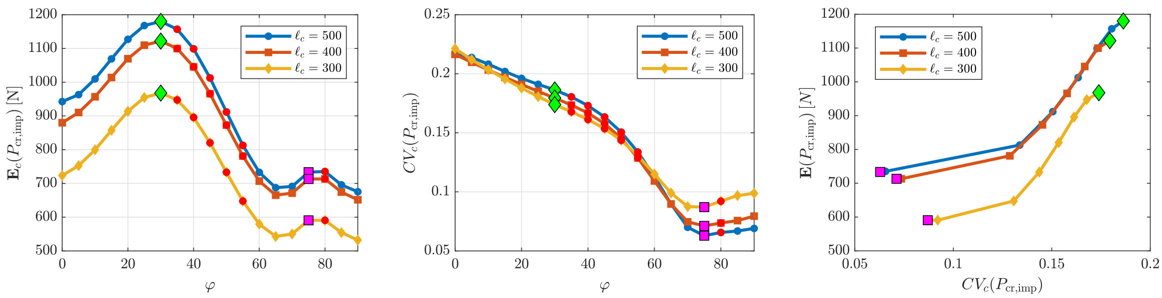

FIGURE 11 | Objective functions (left: performance, middle: robustness, right: Pareto front) for selected correlation length ℓ_c of the fuzzy random field.

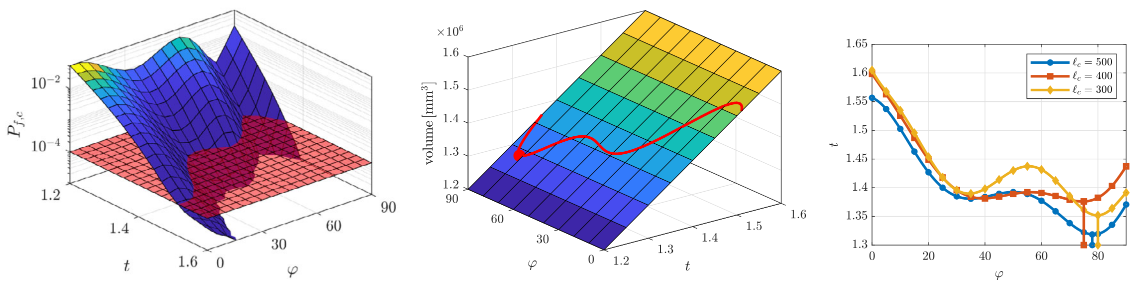

FIGURE 12 | Constraint function (left), objective function with constraint isoline (middle) and constraint isolines for selected correlation lengths (right).

7 | Conclusion

Efficient surrogate modeling is essential for the design optimization of structures with polymorphic uncertainty to reduce computation time. The FNN surrogate model for random fields presented in a previous work has been extended in order to include design and fuzzy input variables. In this way, significant time savings have been achieved. Two different optimization approaches have been investigated in this paper: constraint optimization and multi-objective optimization. It has been shown that the optimal structural design is not trivial, but depends on the preferences between performance, robustness, or reliability. In this example, the optimal design point considering a reliability constraint also achieves robustness but has low performance. In general, the decision-making process can be enhanced, e.g., by utilizing weighted sums of multiple objectives,

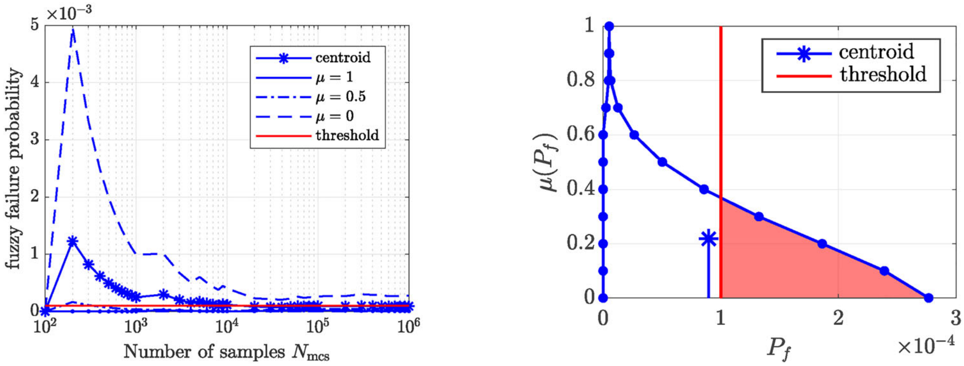

FIGURE 13 | Failure probability for the optimal design point. Convergence plot (left) and fuzzy failure probability (right).

TABLE 1 | Summary of the results for the centroids for the fuzzy mean value and coefficient of variation according to the optimal designs for reliability, performance, and robustness.

	ℓ_c [mm]	t [mm]	φ [°]	$E_c(P_{cr,imp})$ [N]	$CV_c(P_{cr,imp})$ [%]	$P_{f,c}$ [-]
Reliability according to Section 6.3	500	1.319	78	203.9077	8.67	10^{-4}
	400	1.376	75	206.1192	8.73	10^{-4}
	300	1.352	80	107.2537	20.58	10^{-4}
Performance according to Section 6.2	500	2	30	1180.11	18.6324	$<10^{-7}$
	400	2	30	1121.78	17.948	$<10^{-7}$
	300	2	30	967.725	17.3898	$<10^{-7}$
Robustness according to Section 6.2	500	2	75	733.365	6.28692	$<10^{-7}$
	400	2	75	713.127	7.11975	$<10^{-7}$
	300	2	75	590.634	8.70597	$<10^{-7}$

based on their priority, reducing the problem to a single objective optimization.

In this paper, the failure probability is used as a constraint according to design guidelines from civil engineering. Composite materials are widely used in aerospace engineering, and therefore, corresponding design guidelines can have different implications for the optimization problem. The number of design variables is kept low for the sake of simplicity. More design variables can be considered, e.g., independent fiber angles for each layer and multiple thicknesses in stringer stiffened panels. In such a high dimensional design input space, the equidistant sampling method is not efficient and therefore, appropriate optimization algorithms are required. Moreover, some design variables may also be continuous, which would require to combine discrete and continuous optimization approaches. Here, epistemic uncertainty has been taken into account by modeling the standard deviation of the random field describing the geometrical imperfection as a fuzzy variable. Another important random field parameter is the correlation length, which also entails epistemic uncertainty. In this paper, the FNN is trained separately for discrete correlation lengths. The continuous variation of the correlation length involves the solution of the eigenvalue problem of the autocorrelation matrix and, therefore, the variation of eigenvalues and eigenvectors. This would increase the number of input variables, in addition to the random numbers, in an extreme manner. Thus, the development of an efficient surrogate model, able to take the correlation length into account, would be an important extension.

Acknowledgments

Financial support was provided by the Deutsche Forschungsgemeinschaft (DFG, German Research Foundation) in the framework of project 511267658. This support is gratefully acknowledged.

Open access funding enabled and organized by Projekt DEAL.

References

1. B. Budiansky and J. W. Hutchinson, "A Survey of Some Buckling Problems," *AIAA Journal* 4, no. 9 (1966): 1505–1510.

2. V. V. Bolotin, "Statistical Methods in the Nonlinear Theory of Elastic Shells," Presented at a Seminar in the Institute of Mechanics of the Academy of Sciences USSR on 3 October 1957 (Springer-Verlag, 1962).

3. J. Roorda, "Some Statistical Aspects of the Buckling of Imperfection-Sensitive Structures," *Journal of the Mechanics and Physics of Solids* 17, no. 2 (1969): 111–123.

4. V. V. Bolotin, "Statistical Aspects in the Theory of Structural Stability," *Dynamic Stability of Structures* (1967): 67–81.

5. M. Broggi and G. I. Schuëller, "Efficient Modeling of Imperfections for Buckling Analysis of Composite Cylindrical Shells," *Engineering Structures* 33, no. 5 (2011): 1796–1806.

6. C. A. Schenk and G. I. Schuëller, "Buckling Analysis of Cylindrical Shells With Random Geometric Imperfections," *International Journal of Non-Linear Mechanics* 38, no. 7 (2003): 1119–1132.

7. C. A. Schenk and G. I. Schuëller, "Buckling Analysis of Cylindrical Shells With Cutouts Including Random Boundary and Geometric Imperfections," *Computer Methods in Applied Mechanics and Engineering* 196, no. 35–36 (2007): 3424–3434.

8. S. Lauterbach, M. Fina, and W. Wagner, "Influence of Stochastic Geometric Imperfections on the Load-Carrying Behaviour of Thin-Walled Structures Using Constrained Random Fields," *Computational Mechanics* 62, no. 5 (2018): 1107–1125.

9. M. Fina, "Polymorphe Unschärfemodellierung in der nichtlinearen Strukturmechanik - Stabilität von Schalentragwerken, räumliche Variabilität und Metamodellierung" (Diss., Institut für Baustatik, Karlsruher Institut für Technologie, 2020).

10. M. Fina, P. Weber, and W. Wagner, "Polymorphic Uncertainty Modeling for the Simulation of Geometric Imperfections in Probabilistic Design of Cylindrical Shells," *Structural Safety* 82 (2020): 101894.

11. M. Fina, L. Panther, P. Weber, and W. Wagner, "Shell Buckling With Polymorphic Uncertain Surface Imperfections and Sensitivity Analysis," *ASCE-ASME Journal of Risk and Uncertainty in Engineering Systems Part B: Mechanical Engineering* 7, no. 2 (2021): 020909.

12. M. Fina, W. Wagner, and W. Graf, "On Polymorphic Uncertainty Modeling in Shell Buckling," *Computer-Aided Civil and Infrastructure Engineering* 38 (2023): 2632–2647.

13. M. Fina, P. Weber, and W. Wagner, "A Fuzzy Stochastic Correlation Model for Geometric Imperfections of Cylindrical Shells," in *13th International Conference on Applications of Statistics and Probability in Civil Engineering (ICASP13)* (Seoul National University, 2019).

14. M. Fina, P. Weber, and W. Wagner, "Modeling of Aleatory and Epistemic Uncertainties in Probabilistic Design of Cylindrical Shells," in *Proceedings of the 29th European Safety and Reliability Conference (ESREL)* (Research Publishing Services, 2019), 2127–2134.

15. S. Freitag, P. Edler, K. Kremer, and G. Meschke, "Multilevel Surrogate Modeling Approach for Optimization Problems With Polymorphic Uncertain Parameters," *International Journal of Approximate Reasoning* 119 (2020): 81–91.

16. S. Freitag, P. Edler, K. Kremer,M. Hofmann, and G. Meschke, "Optimization Approaches for Durable Reinforced Concrete Structures Considering Interval and Stochastic Parameter Uncertainty," *Proceedings in Applied Mathematics and Mechanics* 18, no. 1 (2018).

17. P. Edler, S. Freitag, K. Kremer, and G. Meschke, "Optimization Approaches for the Numerical Design of Structures Under Consideration of Polymorphic Uncertain Data," *ASCE-ASME Journal of Risk and Uncertaintyin Engineering Systems Part B: Mechanical Engineering* 5, no. 4 (2019): 041013.

18. M. Mäck, I. Caylak, P. Edler, et al., "Optimization With Constraints Considering Polymorphic Uncertainties," *GAMM-Mitteilungen* 42, no. 1 (2019).

19. F. N. Schietzold, W. Graf, and M. Kaliske, "Multi-Objective Optimization of Tree Trunk Axes in Glulam Beam Design Considering Fuzzy Probability-Based Random Fields," *ASCE-ASME Journal of Risk and Uncertainty in Engineering Systems, Part B: Mechanical Engineering* 7, no. 2 (2021).

20. M. Fina, C. Lauff, and W. Wagner, "Optimal Shell Design With Polymorphic Uncertain Parameters," in *8th International Symposium on Reliability Engineering and Risk Management (ISRERM)*, (Research Publishing Services, 2022): 345–349.

21. M. Fina and C. Bisagni, "Buckling Design Optimization of Tow-Steered Composite Panels and Cylindrical Shells Considering Aleatory and Epistemic Uncertainties," *Computational Mechanics* 76 (2025): 59–92.

22. K. Miettinen, F. Ruiz, and A. P. Wierzbicki, *Introduction to Multiobjective Optimization: Interactive Approaches* (Springer, 2008), 27–57.

23. F. Bre and V. D. Fachinotti, "A Computational Multi-Objective Optimization Method to Improve Energy Efficiency and Thermal Comfort in Dwellings," *Energy and Buildings* 154 (2017): 283–294.

24. K. Deb and H. Gupta, "Introducing Robustness in Multi-Objective Optimization," *Evolutionary Computation* 14, no. 4 (2006): 463–494.

25. F. X. Irisarri, F. Laurin, F. H. Leroy, and J. F. Maire, "Computational Strategy for Multiobjective Optimization of Composite Stiffened Panels," *Composite Structures* 93, no. 3 (2011): 1158–1167.

26. S. Rostami, F. Neri, and K. Gyaurski, "On Algorithmic Descriptions and Software Implementations for Multi-Objective Optimisation: A Comparative Study," *SN Computer Science* 1, no. 5 (2020).

27. F. N. Schietzold, F. Leichsenring, M. Götz, W. Graf, and M. Kaliske, "Robustness Versus Performance – Nested Inherence of Objectives in Optimization With Polymorphic Uncertain Parameters," *Advances in Engineering Software* 156 (2021): 102932.

28. M. Fina, C. Lauff, M. G. R. Faes, M. A. Valdebenito, W. Wagner, and S. Freitag, "Bounding Imprecise Failure Probabilities in Structural Mechanics Based on Maximum Standard Deviation," *Structural Safety* 101 (2023): 102293.

29. K. Zhong, J. G. Navarro, S. Govindjee, and G. G. Deierlein, "Surrogate Modeling of Structural Seismic Response Using Probabilistic Learning on Manifolds," *Earthquake Engineering & Structural Dynamics* 52, no. 8 (2023): 2407–2428.

30. V. K. Gudipati and E. J. Cha, "Surrogate Modeling for Structural Response Prediction of a Building Class," *Structural Safety* 89 (2021): 102041.

31. P. Weber, M. Fina, and W. Wagner, "Time Domain Simulation of Earthquake Excited Buildings Using a Fuzzy Stochastic Approach," in *Proceedings of the 29th European Safety and Reliability Conference (ESREL)* (Research Publishing, 2019): 2243–2250.

32. M. Schweizer, M. Fina, W. Wagner, S. Kasic, and S. Freitag, "Uncertain Pedestrian Load Modeling for Structural Vibration Assessment in Footbridge Design," *Engineering Structures* 311 (2024): 118070.

33. M. Fina, M. G. R. Faes, M. A. Valdebenito,W. Wagner, M. Broggi, M. Beer, and S. Freitag, "Estimation of Second-Order Statistics of Buckling Loads Applying Linear and Nonlinear Analysis," in *Proceedings of the 8th International Symposium on Reliability Engineering and Risk Management*, (ISRERM, 2022).

34. M. Fina, M. G. R. Faes, M. A. Valdebenito, et al., "Uncertainty Quantification of Buckling Loads of Thin and Slender Structures Applying Linear and Nonlinear Analysis," in *14th International Conference on Applications of Statistics and Probability in Civil Engineering* (ICASP, 2023).

35. M. Fina, M. A. Valdebenito, W. Wagner, et al., "Control Variates Method to Estimate Stochastic Buckling Loads," *International Journal for Numerical Methods in Engineering* 126, no. 13 (2025): e70070.

36. Z. U. R. Tahir, P. Mandal, M. T. Adil, and F. Naz, "Application of Artificial Neural Network to Predict Buckling Load of Thin Cylindrical Shells Under Axial Compression," *Engineering Structures* 248 (2021): 113221.

37. R. I. Shahin, M. Ahmed, S. A. Yehia, and Q. Q. Liang, "ANN Model for Predicting the Elastic Critical Buckling Coefficients of Prismatic Tapered Steel Web Plates Under Stress Gradients," *Engineering Structures* 294 (2023): 116794.

38. X. He, H. Xu, H. Sabetamal, and D. Sheng, "Machine Learning Aided Stochastic Reliability Analysis of Spatially Variable Slopes," *Computers and Geotechnics* 126 (2020): 103711.

39. X. He, F. Wang, W. Li, and D. Sheng, "Efficient Reliability Analysis Considering Uncertainty in Random Field Parameters: Trained Neural Networks as Surrogate Models," *Computers and Geotechnics* 136 (2021): 104212.

40. P. Hao, Y. Duan, D. Liu, H. Yang, D. Liu, and B. Wang, "Image-Driven Intelligent Prediction of Buckling Behavior for Geometrically Imperfect Cylindrical Shells," *AIAA Journal* 61, no. 5 (2023): 2266–2280.

41. M. Schweizer, M. Fina, W. Wagner, and S. Freitag, "Artificial neural networks for random fields to predict the buckling load of geometrically imperfect structures," *Computational Mechanics* 76 (2025): 181–204.

42. B. Sudret and A. Der Kiureghian, "Stochastic Finite Element Methods and Reliability - A State-of-the-Art Report" (Department of Civil and Environmental Engineering, University of California, 2000).

43. E. Vanmarcke, *Random Fields: Analysis and Synthesis* (MIT Press, 2010).

44. J. Zhang and B. Ellingwood, "Orthogonal Series Expansions of Random Fields in Reliability Analysis," *Journal of Engineering Mechanics* 120, no. 12 (1994): 2660–2677.

45. M. Baitsch, Optimierung Druckbeanspruchter Stabtragwerke Unter Berücksichtigung Geometrischer Imperfektionen (Diss., Ruhr-Universität Bochum, 2003).

46. F. N. Schietzold, A. Schmidt, M. M. Dannert, et al., "Development of 'Development of Fuzzy Probability Based Random Fields for the Numerical Structural Design," *GAMM-Mitteilungen* 42, no. 1 (2019).

47. B. Möller and M. Beer, *Fuzzy Randomness* (Springer, 2004).

48. B. Möller and M. Beer, "EngineeringComputation Under Uncertainty – Capabilities of Non-Traditional Models," *Computers & Structures* 86, no. 10 (2008): 1024–1041.

49. W. Wagner, "A Note on FEM Buckling Analysis," *Communications in Numerical Methods in Engineering* 11, no. 2 (1995): 149–158.

50. R. L. Taylor, FEAP, http://www.ce.berkeley.edu/projects/feap/ (2025).

51. M. Böttcher, W. Graf, and M. Kaliske, "Designing Structures With Polymorphic Uncertainty: Enhanced Decision Making Using Information Reduction Measures to Quantify Robustness," *Proceedings in Applied Mathematics and Mechanics* 23, no. 4 (2023).

52. S. Boyd and L. Vandenberghe, *Convex Optimization* (Cambridge University Press, 2004).

53. M. Beer and M. Liebscher, "Designing Robust Structures – A Nonlinear Simulation Based Approach," *Computers & Structures* 86, no. 10 (2008): 1102–1122.

54. NABau., DIN EN 1990:2021 Eurocode - Basis of Structural and Geotechnical Design (DIN-Normenausschuss Bauwesen (NABau), 2021).

55. B. Möller, W. Graf, and M. Beer, "Fuzzy Structural Analysis Using Alpha-Level Optimization," *Computational Mechanics* 26, no. 6 (2000): 547–565.

56. Z. Gürdal, B. F. Tatting, and C. K. Wu, "Variable Stiffness Composite Panels: Effects of Stiffness Variation on the In-Plane and Buckling Response," *Composites Part A: Applied Science and Manufacturing* 39, no. 5 (2008): 911–922.

57. M. Fina and W. Wagner, "Numerical Stability Analysis With Polymorphic Uncertainty Modelling Under Consideration of Spatial Varying Imperfections," in *Proceedings of the 15th International Probabilistic Workshop & 10th Dresdner Probabilistic Workshop* (TUD press, 2017).